

Time dependent crack tip enrichment for dynamic crack propagation

Thomas Menouillard · Jeong-Hoon Song ·
Qinglin Duan · Ted Belytschko

Received: 8 April 2009 / Accepted: 2 September 2009 / Published online: 29 September 2009
© Springer Science+Business Media B.V. 2009

Abstract We study several enrichment strategies for dynamic crack propagation in the context of the extended finite element method and the effect of different directional criteria on the crack path. A new enrichment method with a time dependent enrichment function is proposed. In contrast to previous approaches, it entails only one crack tip enrichment function. Results for stress intensity factors and crack paths for different enrichments and direction criteria are given.

Keywords Dynamic · Fracture · XFEM

1 Introduction

Classical finite element strategies for dynamic crack propagation simulation are limited because of the evolution of the topology of the crack. They require remeshing after each time step, and also a projection

of the variables on the new discretization. This mandatory process of updating the model is quite costly and awkward. Meshless methods are able to handle such a discontinuity evolution in the structure a lot more easily. [Belytschko et al. \(1996\)](#) proposed meshless approximations based on moving least-squares.

To adapt the standard finite element method to fracture computations, the extended finite element method (XFEM) has been developed, which completely avoids remeshing ([Black and Belytschko 1999](#); [Moës et al. 1999](#)). Also see [Belytschko et al. \(2001\)](#) and [Stolarska et al. \(2001\)](#) where it was combined with level sets. This XFEM method is based on the partition of unity pioneered by [Melenk and Babuška \(1996\)](#), whereby specific functions are used to describe the physical behavior in subdomains of the problem. Thus in [Moës et al. \(1999\)](#), the discontinuous enrichment function was used along the crack in order to describe a discontinuous displacement.

[Belytschko and Chen \(2004\)](#) presented a singular tip enrichment for elastodynamic crack propagation. For plasticity, [Elguedj et al. \(2006\)](#) developed particular functions for elastic-plastic materials for static case. These tip enrichment functions are related to the asymptotic displacement field near the crack tip for such a material law.

[Belytschko et al. \(2003\)](#) developed a method for dynamic crack propagation with loss of hyperbolicity as a propagation criterion. They developed a special element with linear crack opening at the tip. [Moës and Belytschko \(2002\)](#) adapted the cohesive law for

T. Menouillard (✉) · J.-H. Song · Q. Duan · T. Belytschko
Department of Mechanical Engineering, Northwestern
University, 2145 Sheridan Road, Evanston,
IL, 60208-3111, USA
e-mail: t-menouillard@northwestern.edu

J.-H. Song
e-mail: jeonghoonsong2008@u.northwestern.edu

Q. Duan
e-mail: q-duan@northwestern.edu

T. Belytschko
e-mail: tedbelytschko@northwestern.edu

the XFEM method. A lumping technique, based on kinetic energy conservation, to increase the critical time step was studied with XFEM discretization first by Menouillard et al. (2006), Menouillard (2008). Its adaptation to other formulations, such as that of Hansbo and Hansbo (2004), which lead to the phantom node method is given by Song et al. (2006). Rozycki et al. (2008) studied the critical time step within XFEM in explicit dynamic crack propagation with enrichment kept active during the propagation. Linder and Armero (2009) have treated dynamic crack propagation with embedded discontinuity elements.

In this paper, a new method for crack tip enrichment is presented. In addition, we examine the convergence for computed crack paths for the crack tip enrichment methods and compare different crack direction criteria. The new enrichment concept is based on letting the enrichment be a function of time. Consequently, only a single tip enrichment is needed, in contrast to Réthoré et al. (2005). This enrichment also has the advantage that the crack tip inside the element can be modeled.

The presented results show that very accurate stress intensity factors can be computed for stationary cracks. However, for moving cracks, oscillations still occur due to the crack tip moving through an element edge.

This paper is organized as follows; Sect. 2 describes the general mechanical problem of dynamic fracture; it presents the material model, the boundary conditions and the governing equations. Section 3 describes the space discretization of the chosen XFEM method. The fracture mechanics are developed in Sect. 4. Section 5 presents the time discretization corresponding to the Newmark scheme in the explicit case and its stability. Section 6 presents different numerical applications. Section 7 discusses this work and the effective improvements demonstrated in the numerical section.

2 General problem modeling

First we present the general equations for elastodynamic fracture. Let Ω be a bounded cracked domain in \mathbb{R}^2 . (The below also applies in 3D but we only consider 2D problems.)

2.1 Material law

We consider a linear elastic material. The Cauchy stress tensor is denoted by $\underline{\underline{\sigma}}$, the strain tensor $\underline{\underline{\varepsilon}}$, and the material law \mathbb{C} is written as:

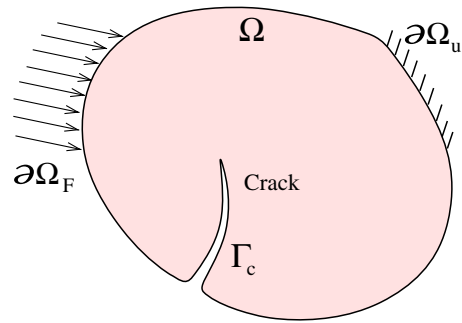


Fig. 1 The cracked domain Ω and its boundaries

$$\underline{\underline{\sigma}}(\mathbf{x}, t) = \mathbb{C} \cdot \underline{\underline{\varepsilon}}(\mathbf{u}(\mathbf{x}, t)) \quad (1)$$

where \mathbf{u} denotes the displacement field. The spatial position is denoted by \mathbf{x} and time by t . The vectors are written in bold and the tensor underlined two times. All the nomenclature is explained in Appendix.

2.2 Boundary conditions

The boundary of the domain Ω is partitioned into $\partial\Omega_u$ on which displacements \mathbf{u}_d are prescribed, $\partial\Omega_F$ on which tractions \mathbf{F}_d are prescribed, and then Γ_c which corresponds to the displacement discontinuity, i.e. crack. One can sum up by writing:

$$\begin{cases} \mathbf{u}(\mathbf{x}, t) = \mathbf{u}_d & \forall \mathbf{x} \in \partial\Omega_u, \forall t \in [1, T] \\ \underline{\underline{\sigma}}(\mathbf{x}, t) \cdot \mathbf{n} = \mathbf{F}_d & \forall \mathbf{x} \in \partial\Omega_F, \forall t \in [1, T] \\ \underline{\underline{\sigma}}(\mathbf{x}, t) \cdot \mathbf{n} = \mathbf{F}_{\text{coh}} & \forall \mathbf{x} \in \partial\Gamma_c, \forall t \in [1, T] \end{cases} \quad (2)$$

where \mathbf{n} denotes outer normal of the boundary, T is the total time. Moreover, the boundary Γ_c also depends on time as the crack propagates: $\Gamma_c(t)$. Note that $\partial\Omega = \partial\Omega_u \cup \partial\Omega_F \cup \Gamma_c$ and $\partial\Omega_u \cap \partial\Omega_F = \emptyset$, $\partial\Omega_u \cap \Gamma_c = \emptyset$, $\partial\Omega_F \cap \Gamma_c = \emptyset$. Figure 1 presents a schematic of the domain Ω and its boundaries where different conditions are applied.

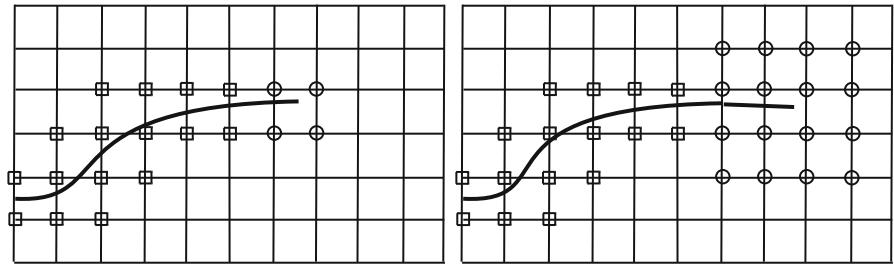
2.3 Momentum equation

The momentum equation is written as:

$$\rho \ddot{\mathbf{u}} = \text{div} \left(\underline{\underline{\sigma}} \right) + \mathbf{f}_d \quad (3)$$

where ρ is the density, and \mathbf{f}_d a force density on the domain Ω . The global equation verified by the displacement solution $\mathbf{u} \in \mathcal{U}$ is (see e.g. Belytschko et al. 2000):

Fig. 2 Squares and circles denote the nodes enriched with the Heaviside step function and the crack tip enrichment function, respectively



$$\begin{aligned}
 & \int_{\Omega/\Gamma_c} \rho \ddot{\mathbf{u}} \cdot \mathbf{v} \, d\Omega + \int_{\Omega/\Gamma_c} \underline{\underline{\sigma}} : \underline{\underline{\varepsilon}}(\mathbf{v}) \, d\Omega \\
 &= \int_{\Omega/\Gamma_c} \mathbf{f}_d \cdot \mathbf{v} \, d\Omega + \int_{\partial\Omega_F} \mathbf{F}_d \cdot \mathbf{v} \, d\Gamma \\
 &+ \int_{\Gamma_c} \mathbf{F}_{coh} \cdot \mathbf{v} \, d\Gamma \tag{4}
 \end{aligned}$$

where $\mathbf{v} \in \mathcal{U}_0$:

$$\mathcal{U} = \{ \mathbf{u} \mid \mathbf{u}(\mathbf{x}) = \mathbf{u}_d, \forall \mathbf{x} \in \partial\Omega_u, \text{ and regularity of } \mathbf{u} \} \tag{5}$$

$$\mathcal{U}_0 = \{ \mathbf{u} \mid \mathbf{u}(\mathbf{x}) = \mathbf{0}, \forall \mathbf{x} \in \partial\Omega_u, \text{ and regularity of } \mathbf{u} \} \tag{6}$$

3 Space discretization and kinematics

3.1 XFEM formulation

A critical part of the formulation is the construction of the displacement field for a crack Γ_c with the crack tip located at $\mathbf{x}_T(t)$. The crack is defined by the signed distance function, where

$$f(\mathbf{x}) = 0 \quad \text{on } \Gamma_c \tag{7}$$

with $f(\mathbf{x}) > 0$ on one side of the crack and $f(\mathbf{x}) < 0$ on the other side. The discrete displacement field \mathbf{u}^h is given by a sum of three parts (see Moës et al. (1999)):

$$\mathbf{u}^h = \mathbf{u}^{cont} + \mathbf{u}^{cut} + \mathbf{u}^{tip} \tag{8}$$

where \mathbf{u}^{cont} is the continuous part of the displacement field, \mathbf{u}^{cut} is the discontinuity across the crack and \mathbf{u}^{tip} is the tip enrichment. For the continuous field, we use the usual finite element approximation

$$\mathbf{u}^{cont}(\mathbf{x}, t) = \sum_{I \in \mathcal{N}} N_I(\mathbf{x}) \mathbf{u}_I(t) \tag{9}$$

where \mathcal{N} is the total number of nodes in the model, $N_I(\mathbf{x})$ are the finite element shape functions and \mathbf{u}_I are the nodal displacements.

The discontinuity across the crack surface is modeled by a discontinuous field which is the second term in Eq. (8) and is given by

$$\mathbf{u}^{cut}(\mathbf{x}, t) = \sum_{I \in \mathcal{N}^{cut}} H(f(\mathbf{x})) N_I(\mathbf{x}) \mathbf{b}_I(t) \tag{10}$$

where \mathbf{b}_I are the additional unknown parameters, often known as enrichment parameters, and $H(\cdot)$ is the Heaviside step function given by

$$H(z) = \begin{cases} 0 & \text{if } z < 0 \\ 1 & \text{if } z \geq 0 \end{cases} \tag{11}$$

and \mathcal{N}^{cut} is the set of enriched nodes associated with the discontinuity. This set of nodes is the set of all nodes of elements cut by the crack Γ_c ; an example of the enrichment scheme is shown in Fig. 2.

The tip enrichment is of the form

$$\mathbf{u}^{tip}(\mathbf{x}, t) = \sum_{I \in \mathcal{N}^{tip}} \phi(\mathbf{x}, t) N_I(\mathbf{x}) \mathbf{e}_I(t) \tag{12}$$

where \mathbf{e}_I are the parameters associated with the tip enrichment and \mathcal{N}^{tip} is the set of nodes at which the tip enrichment are the applied. We have applied tip enrichment in some cases only in the element in which the crack tip currently resides or in a larger domain, such as a 3×3 elements subdomain. These two cases are illustrated in Fig. 2. We have used two types of tip enrichment function:

$$\phi(\mathbf{x}, t) = \|\mathbf{x} - \mathbf{x}_T(t)\|^{\frac{1}{2}} \sin \frac{\theta}{2} \tag{13}$$

$$\phi(\mathbf{x}, t) = \|\mathbf{x} - \mathbf{x}_T(t)\|^2 \sin \frac{\theta}{2} \tag{14}$$

where θ is the angle from the tangent of the crackline to the position of \mathbf{x} as shown in Fig. 3. $\mathbf{x}_T(t)$ denotes the current position of the crack tip.

The first enrichment (see Eq. 13) is the standard singular crack tip field for linear elasticity; it also corresponds to the first function used for enrichment in Fleming et al. (1997) and Moës et al. (1999). The second

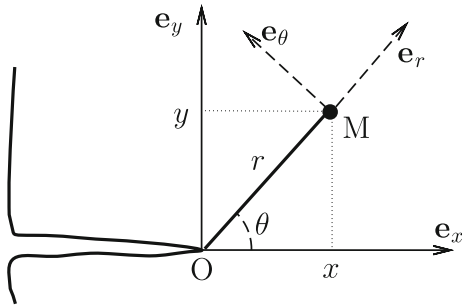


Fig. 3 Cartesian and polar coordinates used near crack tip

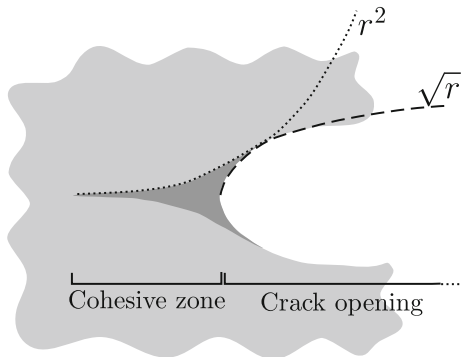


Fig. 4 Displacement zones near crack tip vicinity: discontinuity, and high displacement gradient along the cohesive zone

enrichment is regular and was proposed by Moës and Belytschko (2002) for cohesive models. We will refer to Eq. (13) as the singular enrichment, or $\sqrt{r} \sin(\theta/2)$ enrichment, and to Eq. (14) as the quadratic enrichment, or $r^2 \sin(\theta/2)$ enrichment.

Note that the tip enrichment is time dependent. The position at any time is obtained from the tip velocity, calculated as described later (see Eq. 51). We note that there is only one enrichment function.

The combination of the \mathbf{u}^{cut} and \mathbf{u}^{tip} enrichments enables one to model cohesive cracks as shown in Fig. 4 if a cohesive law is used. The near tip crack opening is quadratic, due to the enrichment, whereas the crack opening further from the tip is modeled by Eq. (12) and depends on the mechanics of the body.

For the nonsingular tip enrichment, i.e. the quadratic one, a cohesive force must be used to model the energy released by the propagation of the crack. The cohesive force law is described later.

3.2 Discrete equations

The discrete equations are obtained via the weak form (see Eq. 4). On developing the equations, we first neglect the time dependence of the tip enrichments. The test function \mathbf{v} is taken to be

$$\mathbf{v}(\mathbf{x}, t) = \sum_{I \in \mathcal{N}} N_I(\mathbf{x}) \mathbf{u}_I(t) + \sum_{J \in \mathcal{N}^{\text{cut}}} H(f(\mathbf{x})) N_J(\mathbf{x}) \mathbf{b}_J(t) + \sum_{K \in \mathcal{N}^{\text{tip}}} \phi(\mathbf{x}, t) N_K(\mathbf{x}) \mathbf{e}_K(t) \quad (15)$$

Substituting the trial function into the weak form (4) gives the following

$$\mathbf{M}_{IJ} \ddot{\mathbf{u}}_J^h = \mathbf{F}_I^{\text{ext}} - \mathbf{F}_I^{\text{int}} + \mathbf{F}_I^{\text{coh}} \quad \forall I \in \mathcal{N} \quad (16)$$

and the remaining terms are defined below:

$$\ddot{\mathbf{u}}^h = \begin{Bmatrix} \ddot{\mathbf{u}}_I \\ \ddot{\mathbf{b}}_I \\ \ddot{\mathbf{e}}_I \end{Bmatrix}, \quad \mathbf{F}_I^{\text{int}} = \begin{Bmatrix} \mathbf{F}_I^{u,\text{int}} \\ \mathbf{F}_I^{b,\text{int}} \\ \mathbf{F}_I^{e,\text{int}} \end{Bmatrix} \quad (17)$$

$$\mathbf{F}_I^{\text{ext}} = \begin{Bmatrix} \mathbf{F}_I^{u,\text{ext}} \\ \mathbf{F}_I^{b,\text{ext}} \\ \mathbf{F}_I^{e,\text{ext}} \end{Bmatrix}, \quad \mathbf{F}_I^{\text{coh}} = \begin{Bmatrix} \mathbf{0} \\ \mathbf{F}_I^{b,\text{coh}} \\ \mathbf{F}_I^{e,\text{coh}} \end{Bmatrix} \quad (18)$$

where

$$\mathbf{F}_{Ii}^{u,\text{int}} = \int_{\Omega} N_{I,j} \sigma_{ji} d\Omega \quad \forall I \in \mathcal{N} \quad (19)$$

$$\mathbf{F}_{Ii}^{b,\text{int}} = \int_{\Omega} N_{I,j} H(f(\mathbf{x})) \sigma_{ji} d\Omega \quad \forall I \in \mathcal{N}^{\text{cut}} \quad (20)$$

$$\mathbf{F}_{Ii}^{e,\text{int}} = \int_{\Omega} (N_I \phi(\mathbf{x}))_{,j} \sigma_{ji} d\Omega \quad \forall I \in \mathcal{N}^{\text{tip}} \quad (21)$$

$$\mathbf{F}_I^{u,\text{ext}} = \int_{\Omega} N_I \mathbf{f}_d d\Omega + \int_{\partial\Omega_F} N_I \mathbf{F}_d d\Gamma \quad \forall I \in \mathcal{N} \quad (22)$$

$$\mathbf{F}_I^{b,\text{ext}} = \int_{\Omega} N_I H(f(\mathbf{x})) \mathbf{f}_d d\Omega + \int_{\partial\Omega_F} N_I H(f(\mathbf{x})) \mathbf{F}_d d\Gamma \quad (23)$$

$$\mathbf{F}_I^{e,\text{ext}} = \int_{\Omega} N_I \phi(\mathbf{x}) \mathbf{f}_d d\Omega \quad (24)$$

$$\mathbf{F}_I^{b,coh} = \int_{\Gamma_c} N_I \mathbf{n} \tau d\Gamma \tag{25}$$

$$\mathbf{F}_I^{e,coh} = \int_{\Gamma_c} N_I \phi(f(\mathbf{x})) \mathbf{n} \tau d\Gamma \tag{26}$$

where τ denotes the opening tensile stress along the crack. The mass matrix is given by

$$\mathbf{M}_{IJ}^{uu} = \int_{\Omega} \rho N_I N_J d\Omega \tag{27}$$

$$\mathbf{M}_{IJ}^{bb} = \int_{\Omega} \rho N_I N_J H^2(f(\mathbf{x})) d\Omega \tag{28}$$

$$\mathbf{M}_{IJ}^{ub} = \int_{\Omega} \rho N_I N_J H(f(\mathbf{x})) d\Omega \tag{29}$$

$$\mathbf{M}_{IJ}^{ee} = \int_{\Omega} \rho N_I N_J \phi^2(\mathbf{x}) d\Omega \tag{30}$$

$$\mathbf{M}_{IJ}^{ue} = \int_{\Omega} \rho N_I N_J \phi(\mathbf{x}) d\Omega \tag{31}$$

$$\mathbf{M}_{IJ}^{be} = \int_{\Omega} \rho N_I N_J H(f(\mathbf{x})) \phi(\mathbf{x}) d\Omega \tag{32}$$

The mass matrix was diagonalized as described in [Menouillard \(2008\)](#). To obtain the equations with the time dependence, we proceed as follows. From Eq. (12), one can evaluate the first and second derivatives in time to compute the velocity and acceleration for the tip enrichment degrees of freedom:

$$\begin{aligned} \dot{\mathbf{u}}^{\text{tip}}(\mathbf{x}, t) &= \sum_{I \in \mathcal{N}^{\text{tip}}} \phi(\mathbf{x}, t) N_I(\mathbf{x}) \dot{\mathbf{e}}_I(t) \\ &\quad + \dot{\phi}(\mathbf{x}, t) N_I(\mathbf{x}) \mathbf{e}_I(t) \end{aligned} \tag{33}$$

$$\begin{aligned} \ddot{\mathbf{u}}^{\text{tip}}(\mathbf{x}, t) &= \sum_{I \in \mathcal{N}^{\text{tip}}} \phi(\mathbf{x}, t) N_I(\mathbf{x}) \ddot{\mathbf{e}}_I(t) \\ &\quad + 2\dot{\phi}(\mathbf{x}, t) N_I(\mathbf{x}) \dot{\mathbf{e}}_I(t) \\ &\quad + \ddot{\phi}(\mathbf{x}, t) N_I(\mathbf{x}) \mathbf{e}_I(t) \end{aligned} \tag{34}$$

Moreover, one can note that as $\phi(\mathbf{x}, t) = \psi(\mathbf{x} - \mathbf{x}_T(t))$, where $\psi(r, \theta)$ is $\sqrt{r} \sin(\theta/2)$ or $r^2 \sin(\theta/2)$, and the derivative of the tip position as a function of time $\dot{\mathbf{x}}_T$ is the crack velocity \mathbf{V}_{tip} :

$$\dot{\phi}(\mathbf{x}, t) = -\dot{\mathbf{x}}_T(t) \nabla \psi \tag{35}$$

$$\ddot{\phi}(\mathbf{x}, t) = -\ddot{\mathbf{x}}_T(t) \nabla \psi - \|\dot{\mathbf{x}}_T(t)\|^2 \nabla^2 \psi \tag{36}$$

where $\mathbf{x}_T(t)$ denotes the crack tip position at time t . Thus, the discrete momentum equation can be written

after reorganizing the different terms, as:

$$\mathbf{M}_{IJ} \ddot{\mathbf{u}}_J^h = \mathbf{F}_I^{\text{ext}} - \mathbf{F}_I^{\text{int}} + \mathbf{F}_J^{\text{coh}} - \mathbf{D}_{IJ}^1 \mathbf{e}_J - \mathbf{D}_{IJ}^2 \dot{\mathbf{e}}_J \tag{37}$$

where $\dot{\mathbf{e}}_J$, \mathbf{e}_J are the degrees of freedom related to the tip enrichment ϕ , and the two matrices \mathbb{D}^1 and \mathbb{D}^2 are defined by:

$$\mathbb{D}^1 = \int_{\Omega} [N, HN, \phi N]^T [N \ddot{\phi}] d\Omega \tag{38}$$

$$\mathbb{D}^2 = \int_{\Omega} [N, HN, \phi N]^T [2N \dot{\phi}] d\Omega \tag{39}$$

Note that these last two matrices depend on the time derivative of the tip enrichment ϕ , and are zero when there is no propagation (i.e. $\dot{\mathbf{x}}_T = 0$).

Only the current crack tip element (or zone) is enriched with the tip enrichment. When the crack tip reaches a new element, the enrichment type of some nodes of this element changes, from ϕ to H , and the degree of freedom corresponding to the Heaviside function has to be initiated. The continuity of the displacement and velocity is chosen for the condition to be verified to initialize the new discontinuous degrees of freedom. With this strategy, the initial value of the new discontinuous enrichment (i.e. corresponding to the H degree of freedom) will not be taken as zero as in [Réthoré et al. \(2005\)](#).

4 Fracture mechanics

4.1 Stress intensity factors

The main step consists in relating the propagation of the crack to the state of the structure, in order to evaluate the direction and velocity of the crack as functions of time: denoted, respectively by $\theta_c(t)$ and $\dot{a}(t)$. The initial value $a(0) = a_0$ is the initial crack length, and the knowledge of the two functions $a(t)$ and $\theta_c(t)$ is sufficient to describe the whole history of the crack geometry in the structure. As we assume that the material is homogeneous with linear isotropic behavior, the problem falls within the framework of the linear dynamic fracture mechanics in which the energy release rate denoted by \mathcal{G} , can be defined. The dynamic stress intensity factors K_1 and K_2 are defined by the asymptotic behavior of the stress near crack tip as in [Bui \(1978\)](#) (see Fig. 3 for coordinates system near crack tip):

$$K_1 = \lim_{r \rightarrow 0} \sqrt{2\pi r} \sigma_{yy} \tag{40}$$

$$K_2 = \lim_{r \rightarrow 0} \sqrt{2\pi r} \sigma_{xy} \tag{41}$$

The relation between the energy release rate and the stress intensity factors is given by Freund (1990) and Bui (1978) as:

$$\mathcal{G} = \frac{1 - \nu^2}{E} \left(\beta_1(\dot{a}) K_1^2 + \beta_2(\dot{a}) K_2^2 \right) \tag{42}$$

where E denotes the Young’s modulus, ν the Poisson’s ratio, \dot{a} the crack velocity, and β_i are the universal functions defined by:

$$\beta_i(\dot{a}) = \frac{4\alpha_i (1 - \alpha_2^2)}{(\kappa + 1)D(\dot{a})} \quad i \in \{1, 2\} \tag{43}$$

$$\alpha_i = \sqrt{1 - \left(\frac{\dot{a}}{c_i}\right)^2} \quad i \in \{1, 2\} \tag{44}$$

$$D(\dot{a}) = 4\alpha_1\alpha_2 - (1 + \alpha_2^2)^2 \tag{45}$$

where c_1 and c_2 are, respectively the dilatational and shear velocities, and are given as a function of the Lamé coefficients and the density as:

$$c_1 = \sqrt{\frac{\lambda + 2\mu}{\rho}}; \quad c_2 = \sqrt{\frac{\mu}{\rho}} \tag{46}$$

The Kolosov coefficient κ is $3 - 4\nu$ for the plane strain, and $(3 - \nu)/(1 + \nu)$ for the plane stress. D is a function whose zero defines the Rayleigh wave celerity denoted by c_r . The dynamic energy release rate predicts a propagation by comparing its value to a critical one \mathcal{G}_c , whereas the knowledge of the stress intensity factors inform about the direction of the propagation. The knowledge of the two stress intensity factors K_1 and K_2 is necessary to evaluate the importance of each mode Bui (1978), and so the new crack direction. The computation of the different stress intensity factors is based on the auxiliary fields near crack tip and the interaction integral which allows to write two scalar equations, and determine the two unknown stress intensity factors K_1 and K_2 ; details of the interaction integral are presented by Freund (1990) and Réthoré et al. (2005).

The stress intensity factors K_1 and K_2 are computed using a domain independent integral I^{int} and a virtual crack extension \mathbf{q} by:

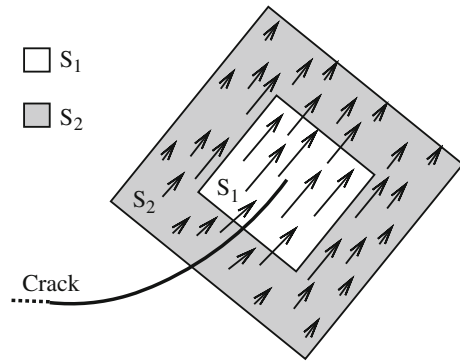


Fig. 5 Direction and norm of the virtual extension field \mathbf{q}

$$\begin{aligned} I^{\text{int}} = & - \int_{\Omega} \left(\underline{\underline{\sigma}}^{\text{aux}} : \underline{\underline{\nabla}}\mathbf{u} - \rho \dot{\mathbf{u}} \underline{\underline{\mathbf{u}}}^{\text{aux}} \right) \text{div}(\mathbf{q}) d\Omega \\ & + \int_{\Omega} \underline{\underline{\sigma}}^{\text{aux}} : \left(\underline{\underline{\nabla}}\mathbf{u} \underline{\underline{\nabla}}\mathbf{q} \right) + \underline{\underline{\sigma}} : \left(\underline{\underline{\nabla}}\mathbf{u}^{\text{aux}} \underline{\underline{\nabla}}\mathbf{q} \right) d\Omega \\ & + \int_{\Omega} \mathbf{div}(\underline{\underline{\sigma}}^{\text{aux}}) \underline{\underline{\nabla}}\mathbf{u}(\mathbf{q}) + \rho \dot{\mathbf{u}} \underline{\underline{\nabla}}\mathbf{u}^{\text{aux}} d\Omega \\ & + \int_{\Omega} \rho \dot{\mathbf{u}}^{\text{aux}} \underline{\underline{\nabla}}\dot{\mathbf{u}}(\mathbf{q}) + \rho \dot{\mathbf{u}} \underline{\underline{\nabla}}\dot{\mathbf{u}}^{\text{aux}}(\mathbf{q}) d\Omega \end{aligned} \tag{47}$$

where $\underline{\underline{\sigma}}^{\text{aux}}$, \mathbf{u}^{aux} are auxiliary stress and displacement fields. The vector \mathbf{q} , parallel to the crack, is defined by:

$$\mathbf{q} = \begin{cases} \mathbf{0} & \text{outside the surface } S_1 \cup S_2 \\ \|\mathbf{q}\| = 1 & \text{inside the surface } S_1 \\ \|\mathbf{q}\| \text{ linear} & \text{inside the surface } S_2 \end{cases} \tag{48}$$

where S_1 and S_2 are surfaces defined near the crack tip. Figure 5 shows the surfaces S_1 and S_2 , and presents the direction and the norm of the virtual extension field \mathbf{q} near the crack tip. Note that the shape of the surfaces S_1 and S_2 can be circular too.

Then this integral is:

$$I^{\text{int}} = \frac{2(1 - \nu^2)}{E} \left(\beta_1(\dot{a}) K_1 K_1^{\text{aux}} + \beta_2(\dot{a}) K_2 K_2^{\text{aux}} \right) \tag{49}$$

The different stress intensity factors are estimated through an appropriate choice of \mathbf{u}^{aux} : i.e. $K_1^{\text{aux}} = 1$ and $K_2^{\text{aux}} = 0$ for the determination of K_1 , and $K_1^{\text{aux}} = 0$ and $K_2^{\text{aux}} = 1$ for the determination of K_2 .

The equivalent dynamic stress intensity factor $K_{\theta\theta}$ is defined by:

$$K_{\theta\theta} = \cos^3\left(\frac{\theta_c}{2}\right) K_1 - \frac{3}{2} \cos\left(\frac{\theta_c}{2}\right) \sin\theta_c K_2 \tag{50}$$

Freund (1972) develops a relation between the dynamic energy release rate and the crack velocity. Freund and Douglas (1982), Freund (1990) and Rosakis and Freund (1982) have linked experimentally, the crack velocity to the stress intensity factors through the relation explained by Freund (1972):

$$\dot{a} = \begin{cases} 0 & \text{if } K_{\theta\theta} < K_{1c}, \\ c_r \left(1 - \left(\frac{K_{1c}}{K_{\theta\theta}} \right)^2 \right) & \text{otherwise.} \end{cases} \quad (51)$$

So a crack increment in the explicit algorithm is defined by $\Delta a = \dot{a} \Delta t$, where Δt is the time step size.

4.2 Fracture criteria

Atluri and Nishioka (1985), Nishioka et al. (1990) classify these different criteria into two categories: explicit and implicit. The explicit one is typically determined by finding the maximum hoop stress as a function of the direction of propagation, and it explicitly leads to the formulation of the direction θ_c as a function of the stress intensity factors.

On this criterion, the angle θ_c is obtained by maximizing the hoop stress near crack tip, which gives Freund (1972):

$$\theta_c = 2 \arctan \left[\frac{1}{4} \left(\frac{K_1}{K_2} - \text{sign}(K_2) \sqrt{8 + \left(\frac{K_1}{K_2} \right)^2} \right) \right] \quad (52)$$

The second category is the implicit criterion, because there is no direct determination of the direction, but an algorithm to determine this direction will converge to it. Thus this direction is determined implicitly. The local symmetry criterion is implicit and requires the crack to propagate in the direction where the mode 2 stress intensity factor vanishes. It is also called “ $K_2 = 0$ ” criterion in Goldstein and Salganik (1974).

In addition, we use a third criterion: the maximum principal strain criterion, in which the direction of crack propagation is normal to the maximum principal strain.

4.3 Cohesive-zone models

An important issue when considering failure is the observation that most engineering materials are not perfectly brittle, but become more ductile after reaching the strength limit. This fracture process zone is

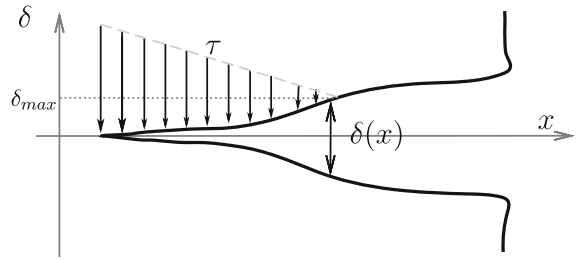


Fig. 6 Cohesive law described with the crack opening δ as a function of the position x along the crack

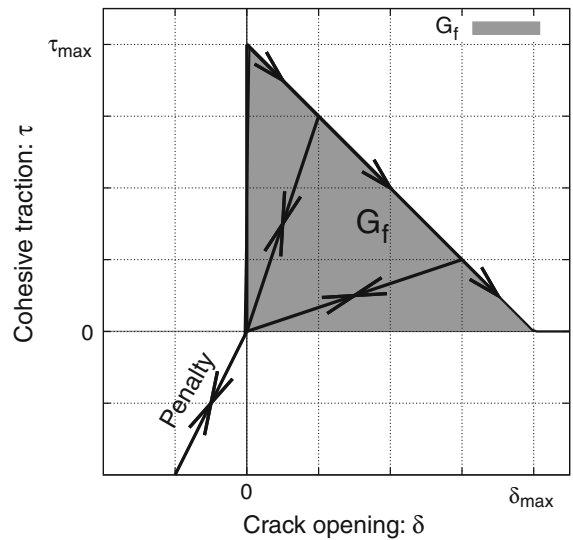


Fig. 7 Linear cohesive law: the area in gray under the curve represents the fracture energy G_f

located in front of the crack tip, and its size characterizes a linear-elastic fracture, or a ductile one. The cohesive forces that exist in this fracture zone need to be taken into account. A good way is to use cohesive-zone models, which were introduced by Barenblatt (1962) for elastic plastic fracture in ductile metals, and by Hillerborg et al. (1976) for brittle materials. Figure 6 shows the crack opening and the tensile stress linked with the position along the crack. It underlines the closing effect near the crack tip and the critical opening δ_{max} ; above this opening, there is no more cohesive stress, because the crack after this point is completely open. Figure 7 presents a linear cohesive law (Song et al. 2006; Rabczuk et al. 2009); the area under the curve represents the fracture energy G_f , defined by:

$$G_f = \int_0^{\delta_{\max}} \tau(\delta) d\delta = \frac{1}{2} \tau_{\max} \delta_{\max} \quad (53)$$

where τ denotes the tensile stress along the crack, and τ_{\max} , δ_{\max} define the linear cohesive law described in Fig. 7.

5 Time integration

5.1 Explicit time integration scheme

The well known form of the explicit Newmark scheme is used:

$$U_{t+\Delta t} = U_t + \Delta t \dot{U}_t + \frac{1}{2} \Delta t^2 \ddot{U}_t \quad (54)$$

$$\dot{U}_{t+\Delta t} = \dot{U}_t + \frac{1}{2} \Delta t (\ddot{U}_t + \ddot{U}_{t+\Delta t}) \quad (55)$$

$$\mathbb{M} \cdot \ddot{U}_{t+\Delta t} = F_{t+\Delta t}^{\text{ext}} - F_{t+\Delta t}^{\text{int}} + F_{t+\Delta t}^{\text{coh}} \quad (56)$$

where U_t , (respectively \dot{U}_t , and \ddot{U}_t) denotes the displacement (respectively velocity, and acceleration) vector as degrees of freedom at time t indicated at the bottom right of the variables. Δt is the time step size, \mathbb{M} the mass matrix, and F^{ext} (respectively F^{int}) the external forces (respectively internal forces) as a vector of degrees of freedom. One has to notice that a diagonal mass matrix is usually used in such a scheme. The advantage is to speed up the computation, and use less memory by storing only vectors instead of matrices.

5.2 Stability of the time integration

The stability condition for such a scheme is defined by a maximal time step size Δt_c , usually named critical time step; a greater time step size used in the computation will not lead to a converged simulation, but to an instability in time. The critical time step is evaluated as:

$$\Delta t_c = \frac{2}{\omega_{\max}} \quad (57)$$

where ω_{\max} denotes the maximum frequency ω determined from the knowledge of the mass \mathbb{M} and stiffness matrix \mathbb{K} by the equation:

$$\det(\mathbb{K} - \omega^2 \mathbb{M}) = 0 \quad (58)$$

The computation frequency must be greater than the greatest vibrational frequency of the structure. The stability in time for the XFEM formulation is defined by the same condition on the mass and the stiffness.

Menouillard et al. (2006) developed a mass lumping strategy for the XFEM formulation, and more particularly for the discontinuous enrichment part. He found that the enrichment does not decrease the stable time step much; indeed the XFEM critical time step is at least 70% of the finite element one. Then, Menouillard (2008) used another decomposition of the enriched shape function developed by Hansbo and Hansbo (2004) which is used in the phantom node method developed by Song et al. (2006). Here, we should make a remark on the critical time step. For the explicit time integration scheme, the critical time step is defined by

$$\Delta t_{\text{crit}} = \frac{2}{\omega_{\max}} \leq \min_{e,I} \frac{2}{\omega_I^e} \quad (59)$$

where ω_I^e is the frequency of element e at node I , and ω_{\max} is the maximum frequency, i.e. maximum eigenvalue, of the linearized system $\omega^2 \mathbb{M} = \mathbb{K}$: i.e. ω is the solution of Eq. (58). Note that the critical time step of an XFEM mesh is bounded by the critical time step of the cracked element: for details, refer to Song et al. (2006) and Menouillard et al. (2006), Menouillard (2008).

Similarly, the critical time step of the proposed method is also bounded by that of cracking nodes. One obtains then

$$\begin{aligned} & \det(\mathbb{K}^{\text{xfem}} - \omega^2 \mathbb{M}^{\text{xfem,lump}}) \\ &= \frac{A_I}{A} \det(\mathbb{K}^{\text{fem}} - \omega^2 \mathbb{M}^{\text{fem,lump}}) = 0 \end{aligned} \quad (60)$$

As we can see from Eq. (60), the area fraction is factored out and then the linearized system equation of cracked elements can be replaced with the linearized system equation of continuum elements. Menouillard (2008) showed that the critical time step of the cracked element is the same as that of the continuum element and underlined that this is true for any elements with shape function with constant gradients; in others words in any constant strain elements such as 3-node linear element. Whereas the 4-node linear element is not a constant strain element, the latter relation holds approximately because this element as been used with one quadrature point and hourglass control Flanagan and Belytschko (1981), Koh and Kikuchi (1987); so it becomes like a constant strain element Liu et al. (1994).

The critical time step due to the XFEM formulation and more particularly to the tip enrichment function was studied by Elguedj et al. (2009), using the same approach as the one used with the discontinuous enrichment in Menouillard (2008), applied to

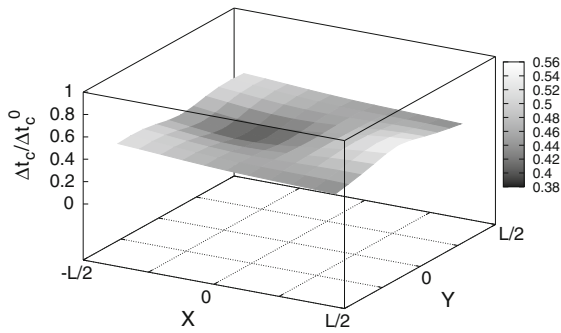


Fig. 8 Normalized critical time step for the tip element with the enriched function $r^2 \sin(\theta/2)$

the tip enrichment $\sqrt{r} \sin(\theta/2)$. The development of the lumped mass matrix is based on the conservation of the discretized kinetic energy. The critical time step is thus not penalizing compared to the one of the non-enriched element. Thus, Fig. 8 presents the normalized critical time step for a quadrilateral element with the $r^2 \sin(\theta/2)$ tip enrichment for an horizontal crack from the edge point $(-L/2, Y)$ to the crack tip (X, Y) . It shows the time step is affected by the position of the crack in the element, but the critical time step is at least 40% of the uncracked finite element.

The stability study of the Newmark scheme has been developed with the XFEM formulation with the kinds of tip enrichment which will be used here.

6 Numerical examples

This section presents several numerical applications which examine the performance for various tip enrichments and global paths in crack propagation. The accuracy of the computation of the stress intensity factors is studied through three numerical applications: a stationary mixed mode crack, and a stationary and moving crack in mode I. The use of different tip enrichments in the XFEM discretization is discussed. Then, a numerical application in mixed mode crack propagation is computed with different tip enrichments, and the improvement of the use of tip enrichment is discussed for propagating crack. Furthermore, the convergence of the crack path with mesh refinement is studied.

6.1 Stationary mixed mode crack

This example deals with a stationary mixed mode crack, and focuses on the computation of the two dynamic

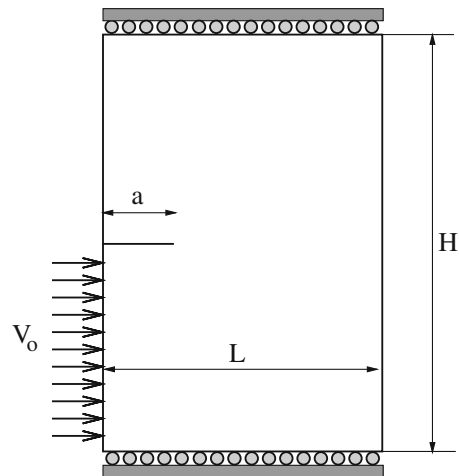


Fig. 9 Geometry and loading

Table 1 Material properties for the mode 2 semi infinite plate test

Material property	Symbol	Value
Young’s modulus	E	200 GPa
Poisson’s ratio	ν	0.25
Density	ρ	7,833 kg/m ³

stress intensity factors, K_1 and K_2 . Figure 9 presents the geometry and the loading. The dimensions are the following: $H = 6$ m, $a = 1$ m, and $L = 4$ m. The prescribed velocity on the boundary is $V_0 = 16.5$ m/s. Two meshes are used: 40×59 and 60×119 4-node elements. The material model is linear elastic, and the properties are given in Table 1. An analytical solution for both stress intensity factors as a function of time is available for this problem Lee and Freund (1990), Ravi-Chandar (2004). The numerical results are valid only until the compressive stress wave reaches again the crack tip after having been reflected on the right edge of the structure. The time needed for the wave to first reach the crack tip is given by $t_c = a_0/c_1$. Then, the computation is run until $3 t_c$. The stress intensity factors are normalized by $\frac{-E V_0 \sqrt{a/\pi}}{2 c_1 (1-\nu^2)}$. In all of the results, “no tip” refers to the case when the crack was represented with only the Heaviside function enrichment (see Eq. 10).

Figure 10 presents the two normalized stress intensity factors K_1 and K_2 as a function of time for different tip enrichments: $\sqrt{r} \sin(\theta/2)$ and $r^2 \sin(\theta/2)$, computed for the coarse mesh (40×59 elements). The analytical solution and the computation without tip enrichment are illustrated in Fig. 10. For these

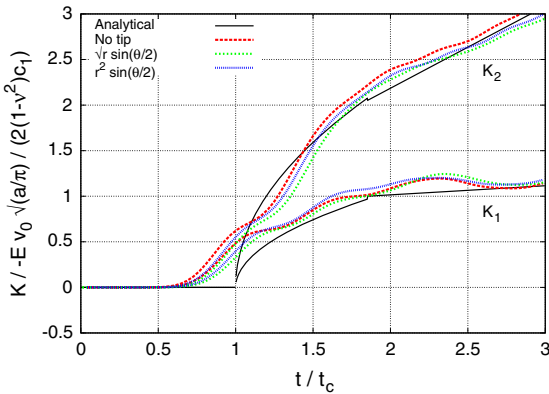


Fig. 10 Normalized stress intensity factors as a function of the time for the discretization 40×59 elements

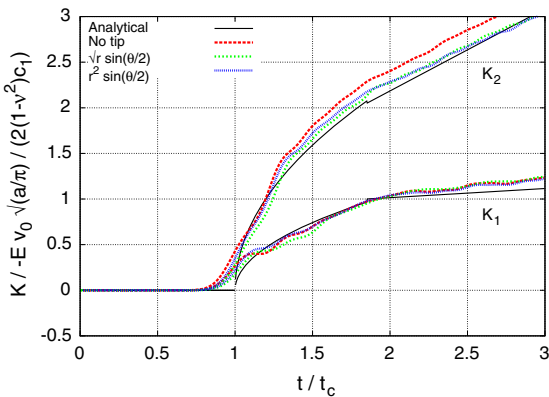


Fig. 11 Normalized stress intensity factors as a function of the time for the discretization 60×119 elements

computations, the tip enrichment is only placed on the four nodes of the tip element. For the coarse mesh results (40×59) in Fig. 10, the errors for all three enrichments are substantial except at late times. The singular enrichment is the best. The Heaviside enrichment (“no tip”) is the worst but is still surprisingly good. One can notice in Fig. 10, that the use of tip enrichment (even $r^2 \sin(\theta/2)$) gives an improvement on the computation of the stress intensity factors over the Heaviside enrichment. According to the material law and fracture mechanics framework, the superiority of the singular enrichment is expected.

Figure 11 presents the normalized stress intensity factors as a function of time computed for the fine mesh (i.e. 60×119 elements). The results of different tip enrichments (i.e. $\sqrt{r} \sin(\theta/2)$, $r^2 \sin(\theta/2)$) are compared to XFEM discretization without tip enrichment and the analytical solution.

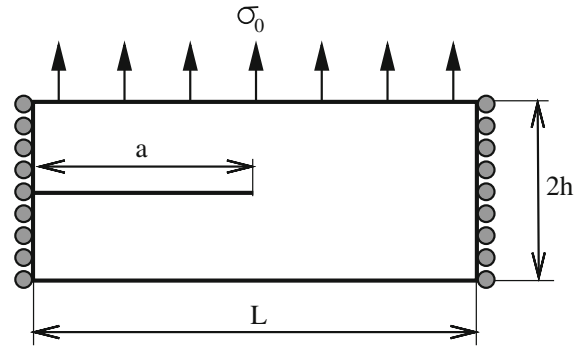


Fig. 12 Geometry and loading for the infinite plate example

The numerical results again show good agreement with the analytical solution. Inexplicably the computation with only the Heaviside enrichment gets worse for the finer mesh, so perhaps the good accuracy for the coarse mesh solution is serendipitous. However, the results with a tip enrichment are closer to the analytical solution than the one without tip enrichment. The singular enrichment ($\sqrt{r} \sin(\theta/2)$) gives the results closest to the analytical solutions.

6.2 Stationary and moving mode 1 crack

The example considered in this paragraph is an infinite plate with a semi infinite crack [Ravi-Chandar \(2004\)](#) loaded as shown in Fig. 12. A theoretical solution of this problem for a given crack velocity is given in [Freund \(1990\)](#). Since this analytical solution was obtained under the assumptions of an infinite plate with a semi-infinite crack and a given speed of the crack’s tip, according to the geometry described in Fig. 12, those could be compared for time $t \leq 3t_c = 3h/c_1$ (where c_1 is the dilatational wave speed). Beyond that, the reflected stress wave reaches the crack tip and the analytical solution is no longer valid. The dimensions are the following: the length $L = 10$ m, the initial crack length $a = 5$ m, and the vertical position of the crack is $h = 2$ m. Two regular meshes are used: 78×39 and 120×59 4-node elements. The material properties of the linear elastic media are given in Table 2. The tensile stress applied on the top surface is $\sigma_0 = 500$ MPa. Two different simulations are performed here: the first one with a stationary crack and the second one with a moving crack driven by an imposed velocity of the crack tip. The stress intensity factor in mode 1 is normalized by $\sigma_0 \sqrt{h}$.

Table 2 Material properties for the stationary and moving crack experiment in pure mode I

Material property	Symbol	Value
Young’s modulus	E	210 GPa
Poisson’s ratio	ν	0.3
Density	ρ	8,000 kg/m ³

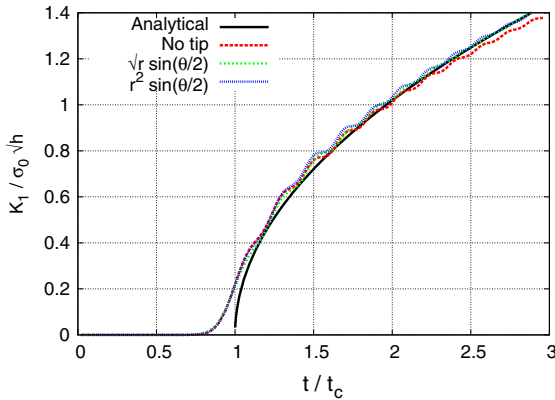


Fig. 13 Normalized stress intensity factor as a function of the time for several kinds of enrichment for stationary crack in Fig. 12 (no tip enrichment, $\sqrt{r} \sin(\theta/2)$, $r^2 \sin(\theta/2)$) and the coarse mesh (78×39)

6.2.1 Stationary crack

As the tensile wave reaches the crack at time t_c , the mode I stress intensity factor can be written as:

$$K_I(0, t) = \begin{cases} 0 & \text{if } t < t_c \\ \frac{2\sigma_0}{1-\nu} \sqrt{\frac{c_1(t-t_c)(1-2\nu)}{\pi}} & \text{if } t \geq t_c \end{cases} \quad (61)$$

Figure 13 presents the normalized stress intensity factor as a function of time for the coarse mesh (78×39 elements). One notices that the results for the different enrichments (singular or quadratic) match the analytical solution closely. The error near $t = t_c$ is due to the tensile stress wave entering the contour for the stress intensity factor computation (i.e. interaction integral) before it reaches the crack tip. As shown in Fig. 14, a finer mesh gives better results near $t = t_c$, because a smaller contour can be used with the same number of elements. Figure 15 presents the relative error in term of stress intensity factor obtained for the fine mesh. It shows that the best results are given by the computations using tip enrichment, and more particularly the singular enrichment. The errors are quite large, especially when no tip enrichment is used. Figure 16

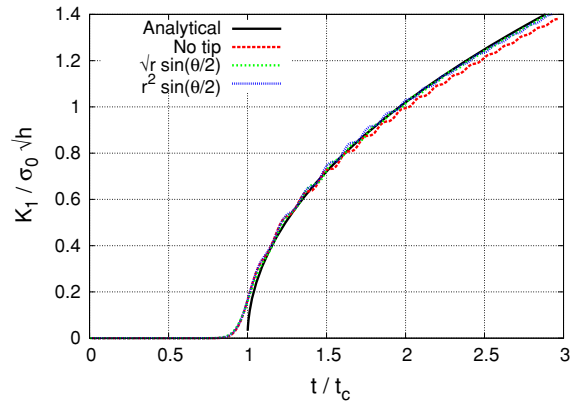


Fig. 14 Normalized stress intensity factor as a function of the time for several kinds of enrichment for stationary crack in Fig. 12 (no tip enrichment, $\sqrt{r} \sin(\theta/2)$, $r^2 \sin(\theta/2)$) and the coarse mesh (120×59)

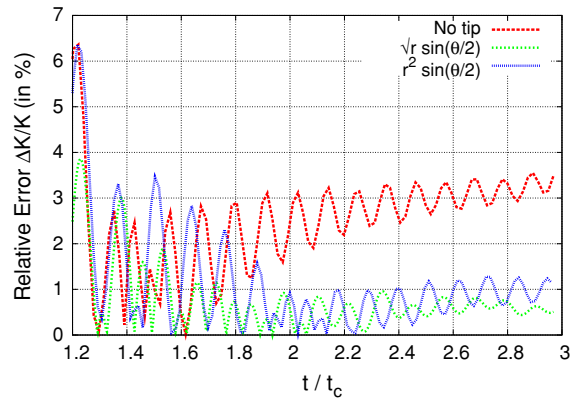


Fig. 15 Relative error on stress intensity factor as a function of the time for 3 kinds of enrichment for stationary crack in Fig. 12 (no tip enrichment, $\sqrt{r} \sin(\theta/2)$ and $r^2 \sin(\theta/2)$) and the fine mesh (120×59 elements)

presents the results obtained with a 3 by 3 enriched elements domain. It underlines the previous statement.

6.2.2 Moving crack

Let us study the effect of a moving crack on the computation of the stress intensity factor and the use of tip enrichment. The crack velocity is imposed to be zero until $1.5 t_c$, and 1,500 m/s after. For the moving crack in this pure mode I test, the stress intensity factor can be written as given in Freund (1990) in the form:

$$K_I(\dot{a}, t) = \gamma(\dot{a}) K_I(0, t) \quad (62)$$

where $K_I^{\text{dyn}}(0, t)$ is the previous stress intensity factor corresponding to the static crack, and γ is an universal

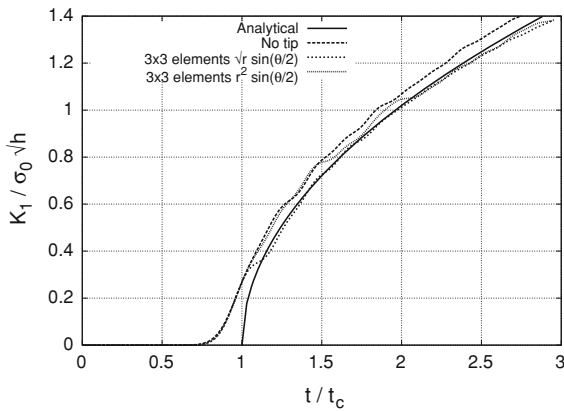


Fig. 16 Normalized stress intensity factor as a function of the time for several kinds of enrichment for stationary crack in Fig. 12 ($r \sin(\theta/2)$, $r^2 \sin(\theta/2)$) in a 3 by 3 elements zone near crack tip

function of the crack velocity \dot{a} , which can be approximated by:

$$\gamma(\dot{a}) = \frac{1 - \frac{\dot{a}}{c_r}}{1 - \frac{\dot{a}}{2c_r}} \quad (63)$$

where $c_r = 2,947$ m/s and $c_1 = 5,944$ m/s. So, one has the relation between the stress intensity factor K_I and the velocity \dot{a} of the crack:

$$K_I(\dot{a}, t) = \begin{cases} 0 & \text{if } t < t_c \\ \frac{2\sigma_0}{1-\nu} \sqrt{\frac{c_1(t-t_c)(1-2\nu)}{\pi}} & \text{if } t_c \leq t < 1.5t_c \\ \frac{2\sigma_0}{1-\nu} \sqrt{\frac{c_1(t-t_c)(1-2\nu)}{\pi}} \frac{1-\frac{\dot{a}}{c_r}}{1-\frac{\dot{a}}{2c_r}} & \text{if } 1.5t_c \leq t \end{cases} \quad (64)$$

Figure 17 presents the stress intensity factor K_I normalized as a function of time with different tip enrichment and compared to the analytical solution for the fine mesh, whereas Fig. 18 shows the results for the coarse mesh (78×39). To underline the effect of the tip enrichment, Fig. 19 presents the relative error during the crack propagation for the different tip enrichments for the fine mesh. It can be seen that the use of the enrichment (singular or quadratic) decreases the error during the propagation phase of the simulation, but the best result is obtained with the quadratic enrichment for the moving crack. One can conclude for this example with crack propagation, that the use of a tip enrichment improves the results of the stress intensity factor computation by decreasing the oscillations during the crack

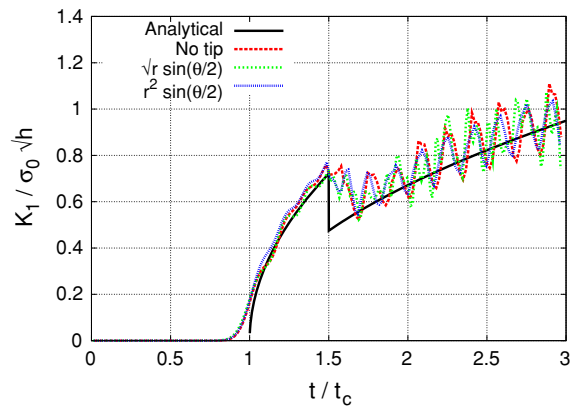


Fig. 17 Normalized stress intensity factor as a function of the time for 3 kinds of enrichment for moving crack in Fig. 12 (no tip enrichment, $\sqrt{r} \sin(\theta/2)$ and $r^2 \sin(\theta/2)$) and the fine mesh (120×59 elements)

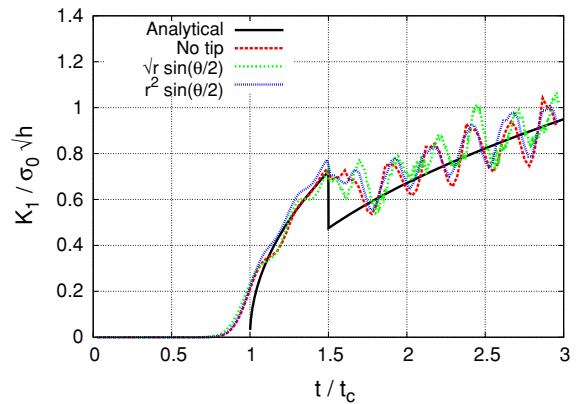


Fig. 18 Normalized stress intensity factor as a function of the time for 3 kinds of enrichment for moving crack in Fig. 12 (no tip enrichment, $\sqrt{r} \sin(\theta/2)$ and $r^2 \sin(\theta/2)$) and the coarse mesh (78×39 elements)

propagation. However the errors are still unacceptably large. The oscillations correspond to the crack tip passing from one element to the next. The enrichment does not decrease this error significantly. This error was also strongly apparent in the multi-enrichment technique of Réthoré et al. (2005), Elguedj et al. (2009).

The same computation has been performed by enlarging the tip enrichment zone from 1 element to 3 by 3 elements around the crack tip. Figure 20 presents the stress intensity factor K_I normalized as a function of time with different tip enrichments and compared to the analytical solution. One can notice that the oscillations are significantly reduced by enlarging the tip enrichment region. The oscillations may perhaps be

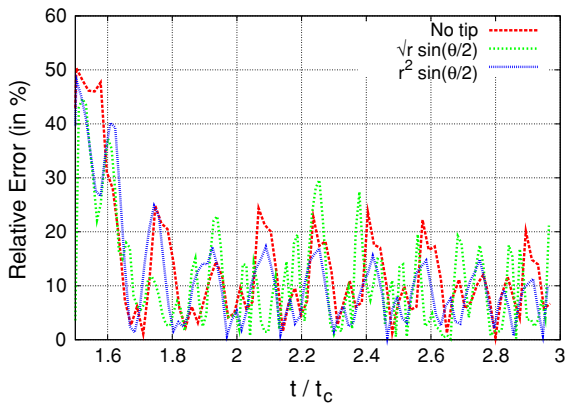


Fig. 19 Relative error on stress intensity factor as a function of the time for 3 kinds of enrichment for moving crack in Fig. 12 (no tip enrichment, $\sqrt{r} \sin(\theta/2)$ and $r^2 \sin(\theta/2)$) and the fine mesh (120×59 elements)

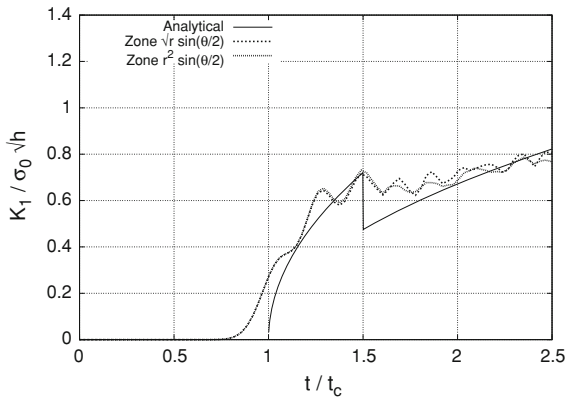


Fig. 20 Normalized stress intensity factor as a function of the time for 3 kinds of enrichment for moving crack in Fig. 12 (no tip enrichment, $\sqrt{r} \sin(\theta/2)$ and $r^2 \sin(\theta/2)$) and the coarse mesh (78×39 elements); the particularity is that a zone (3 by elements) near crack tip is enriched

further reduced by going to smoother interpolants, such as in K -methods.

6.3 Kalthoff's experiment

This example is based on the experiment of Kalthoff (1985) and by Böhme and Kalthoff (1982) and deals with the crack propagation initially in mode 2. A plate with two symmetrical edge cracks is impacted by a projectile at speed V_0 . The two cracks are centered with respect to the specimen's geometry and their separation corresponds to the diameter of the projectile. The crack propagates with an overall angle from 60° to 70° .

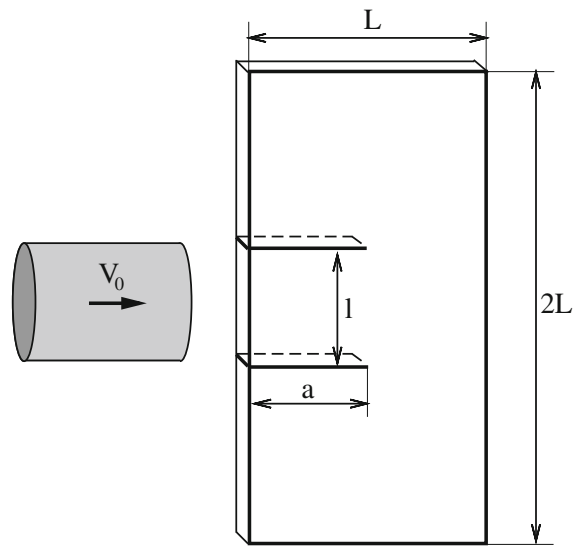


Fig. 21 Geometry of the Kalthoff's experiment

Table 3 Material properties for the Kalthoff's experiment

Material property	Symbol	Value
Young's modulus	E	190 GPa
Poisson ratio	ν	0.3
Density	ρ	$8,000 \text{ kg/m}^3$
Fracture toughness	K_{Ic}	$68 \text{ MPa} \sqrt{\text{m}}$

We chose $V_0 = 20 \text{ m/s}$ as a typical velocity for brittle fracture. A schematic description of the problem and the geometry is given by Fig. 21. The dimensions of the specimen are: $L = 100 \text{ mm}$, $l = 50 \text{ mm}$, $a = 50 \text{ mm}$ and the thickness is 16.5 mm . The material properties of the linear elastic media in plane strain are given in Table 3. A cohesive zone model as presented in Sect. 4.3 is used in this example, with $G_F = 22, 146.5 \text{ Pa}\cdot\text{m}$.

This problem is widely used to validate numerical methods in dynamic crack propagation. For the particular case of the extended finite element method, the interest is in the fact that whereas the mesh is structured, the crack propagates with an angle of 60° – 70° , so the crack path does not respect the orientation of the mesh, i.e. it is not parallel to any element edges. However, no studies of the effects of the fracture direction criterion or the convergence of the crack path have been made heretofore.

Regular meshes (22×22 , 38×38 , 78×78 and 198×198) with 4-node elements were employed in the simulations. Computations were run with different tip

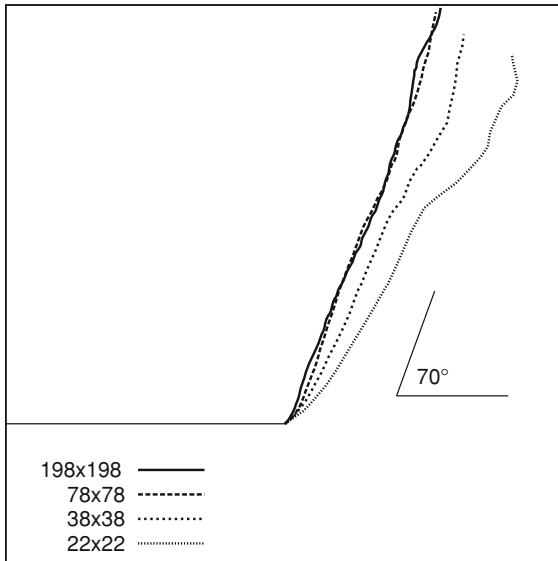


Fig. 22 Crack paths of the Kalthoff test with the maximum strain criterion for 4 different meshes: 198×198 , 78×78 , 38×38 and 22×22

enrichments: no tip enrichment (i.e. only the Heaviside discontinuity), singular enrichment (i.e. $\sqrt{r} \sin(\theta/2)$) and quadratic enrichment (i.e. $r^2 \sin(\theta/2)$). The crack velocity is driven by Eq. (51).

Figure 22 presents results for the four meshes for the principal strain criterion. It can be seen that while there are significant differences between the three coarse meshes, the two finest are almost identical. Thus that path can be considered as a converged solution. The angle is 70° .

Figure 23 presents the crack lengths as a function of time for the 22×22 and 78×78 element meshes with different tip enrichments: no enrichment, singular and quadratic enrichment. These figures show similar results for the crack tip velocity, which is the slope of the curve, for the different meshes and tip enrichments.

Figure 24 shows the influence of the tip enrichment with the three different meshes. It can be seen that the paths for the two coarser meshes are quite different. However, the two paths for the two finer meshes are almost identical, indicating convergence. However, the converged path required a very fine mesh, much finer than in static growth Moës and Belytschko (2002). The converged path is almost straight and at an angle of 70° with the horizontal.

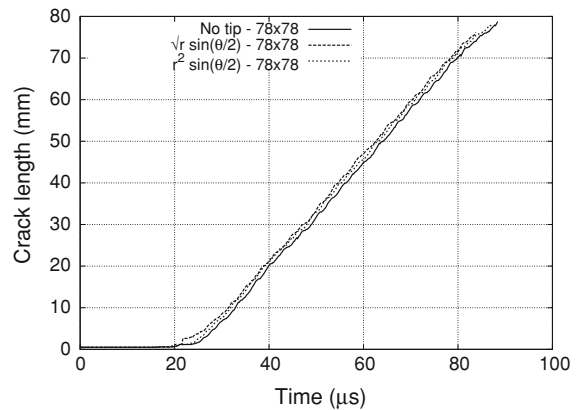
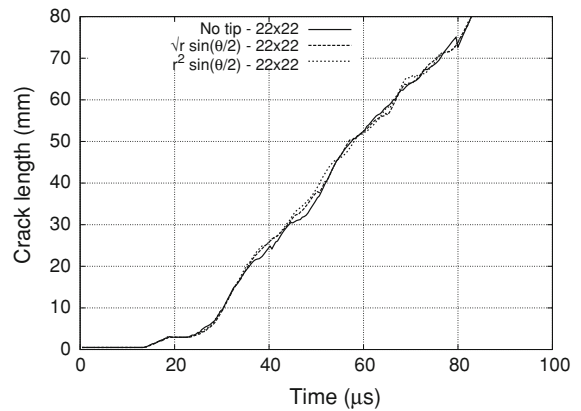


Fig. 23 Crack lengths of the Kalthoff test with different tip enrichments for the 22×22 and 78×78 element mesh

These results show that the use of a tip enrichment tends to have the same effect as using a finer mesh, because it tends to make the crack path closer to the 70° angle, but the effect on the crack length as a function of time is not so important as shown in Fig. 23. In addition, one can notice that the tip enrichment smoothes the crack path compared to the no tip enrichment case. We found the results obtained with the local symmetry criterion (“ $K_2 = 0$ ”) and the maximum hoop stress criterion (see Eq. 52) were very similar, so only the maximum hoop stress criterion is presented.

Figure 25 presents the crack paths for finer meshes according to strain criterion and maximum principal strain: it underlines the agreement between the two criteria for a fine mesh. One notices that the results obtained with the two criteria (local maximum strain or global maximum hoop stress) are similar for a given mesh. Also, the finer the mesh, the closer to 70° the angle of the crack path for both criteria.

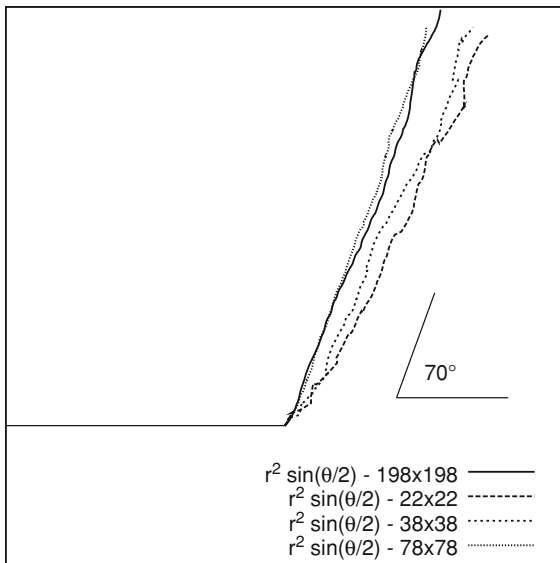
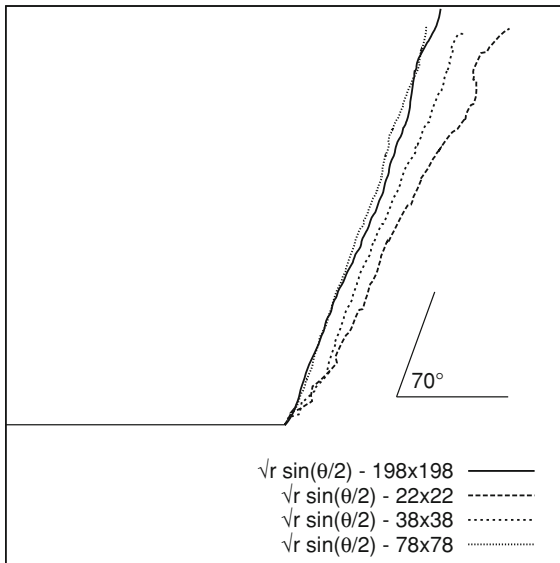


Fig. 24 Crack paths for different tip enrichments ($\sqrt{r} \sin(\theta/2)$ and $r^2 \sin(\theta/2)$) with the maximum hoop stress criterion, and different meshes (22×22 , 38×38 and 78×78)

7 Conclusion

A new enrichment method has been proposed for the extended finite element method. In this method, the Heaviside function enrichment is used along the crack, and a single time-dependent tip enrichment function is used around the crack tip. The two kinds of tip enrichments investigated in this study are the singular

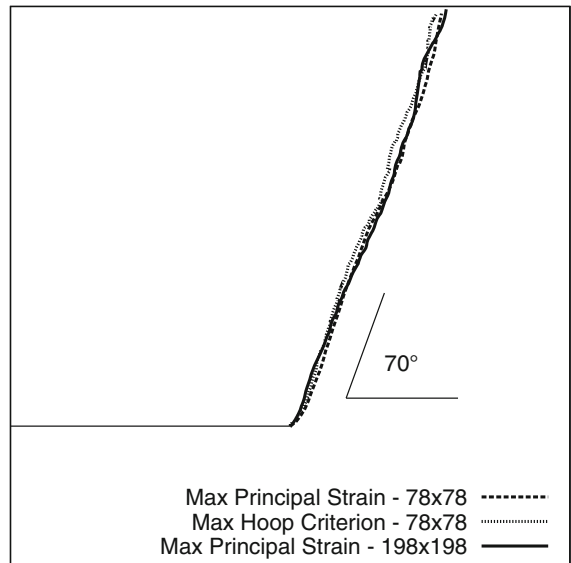


Fig. 25 Crack paths for different criteria: maximum hoop stress criterion and local maximum principal strain, with the fine mesh

(i.e. $\sqrt{r} \sin(\theta/2)$) and the quadratic (i.e. $r^2 \sin(\theta/2)$) enrichments.

For a stationary crack, both tip enrichments improve the accuracy of the stress intensity factors. In particular, the singular enrichment gives the best results, and they agree very closely with analytical solutions.

For a moving crack, oscillations occur on the stress intensity factors. They correspond to the crack tip passing from one element to the next. Even though the tip enrichments slightly decrease their amplitude, the errors remain significant (i.e. up to 20%). Overcoming this accuracy requires further study.

The convergence of crack paths for paths at arbitrary skewed angles was also studied. The study of crack paths by means of the Kalthoff experiment shows that the convergence in term of crack path is reached for a 78 by 78 element mesh. Moreover, the three fracture criteria (local maximum principal strain, maximum hoop stress and local symmetry criterion) converge to the same path with a fine mesh; it exactly corresponds to a 70° angle. In addition, the use of tip enrichment tends to have the same effect as mesh refinement because it improves the results for coarse meshes.

Acknowledgments The support of the Office of Naval Research under Grants N00014-08-C-0592 and N00014-03-1-0097 is gratefully acknowledged.

Nomenclature

Notation	Meaning
Ω	Domain
$t, \Delta t, \Delta t_c$	Time, time step and critical time step
\mathbf{x}	Spatial coordinates
\mathbf{x}_T	Crack tip position
$\mathbf{u}, \dot{\mathbf{u}}, \ddot{\mathbf{u}}$	Displacement, velocity, acceleration
$\underline{\underline{\sigma}}$	Cauchy stress tensor
$\underline{\underline{\varepsilon}}$	Strain tensor
\mathbb{C}	Hook law
U, \dot{U}, \ddot{U}	Displacement, velocity, acceleration
\mathbb{M}, \mathbb{K}	Mass, stiffness matrices
$F^{\text{ext}}, F^{\text{int}}$	External and internal forces
\mathbf{u}^h	Discretized displacement
N_I	Shape function
H	Heaviside function
f	Level set (crack surface)
ϕ	Tip enrichment function
r, θ	Polar coordinates near crack tip
u_I, b_I, e_I	Degrees of freedom in XFEM
ρ	Density
E	Young's modulus
ν	Poisson's ratio
ω	Frequency
κ	Kolosov's coefficient
c_1, c_2	Dilatation, shear wave velocities
c_r	Rayleigh wave velocity
α_1, α_2	Crack velocity functions
β_1, β_2	Universal functions
K_1, K_2	Dynamic stress intensity factors
K_{1c}	Critical stress intensity factors
$K_{\theta\theta}$	Equivalent stress intensity factor
\mathcal{G}	Energy release rate
G_f	Fracture energy
a, \dot{a}	Crack length, and velocity
θ_c	Crack turning angle
V_0	Velocity

References

- Atluri SN, Nishioka T (1985) Numerical studies in dynamic fracture mechanics. *Int J Frac* 27(3):245–261
- Barenblatt GI (1962) The mathematical theory of equilibrium cracks formed in brittle fracture. *Adv Appl Mech* 7:55–129

- Belytschko T, Chen H (2004) Singular enrichment finite element method for elastodynamic crack propagation. *Int J Comput Method* 1(1):1–15
- Belytschko T, Chen H, Xu J, Zi G (2003) Dynamic crack propagation based on loss of hyperbolicity and a new discontinuous enrichment. *Int J Numer Method Engin* 58:1873–1905
- Belytschko T, Krongauz Y, Organ D, Fleming M, Krysl P (1996) Meshless methods: an overview and recent developments. *Comput Method Appl Mech Engin* 139(1–4):3–47
- Belytschko T, Liu WK, Moran B (2000) *Nonlinear finite elements for continua and structures*. Wiley, Chichester
- Belytschko T, Moës N, Usui S, Parimi C (2001) Arbitrary discontinuities in finite elements. *Int J Numer Method Engin* 50(4):993–1013
- Black T, Belytschko T (1999) Elastic crack growth in finite elements with minimal remeshing. *Int J Numer Method Engin* 45:601–620
- Böhme W, Kalthoff JF (1982) The behavior of notched bend specimens in impact testing. *Int J Frac* 20(4):139–143
- Bui HD (1978) *Mecanique de la rupture fragile*. Masson, Paris
- Elguedj T, Gravouil A, Combescure A (2006) Appropriate extended functions for X-FEM simulation of plastic fracture mechanics. *Comput Method Appl Mech Engin* 195(7–8):501–515
- Elguedj T, Gravouil A, Maigre H (2009) An explicit dynamics extended finite element method. part 1: mass lumping for arbitrary enrichment functions. *Comput Method Appl Mech Engin* 198(30–32):2297–2317
- Flanagan DP, Belytschko T (1981) A uniform strain hexahedron and quadrilateral with orthogonal hourglass control (in one-point integration of isoparametric finite element analysis). *Int J Numer Method Engin* 17:679–706
- Fleming M, Chu YA, Moran B, Belytschko T (1997) Enriched element-free Galerkin methods for crack tip fields. *Int J Numer Method Engin* 40(8):1483–1504
- Freund LB (1972) Crack propagation in an elastic solid subjected to general loading. Pt. 1. Constant rate of extension. *J Mech Phys Solid* 20(3):129–140
- Freund LB (1990) *Dynamic fracture mechanics*. Cambridge University Press, Cambridge
- Freund LB, Douglas AS (1982) Influence of inertia on elastic-plastic antiplane-shear crack growth. *J Mech Phys Solid* 30(1):59–74
- Gol'dstein RV, Salganik RL (1974) Brittle fracture of solids with arbitrary cracks. *Int J Frac* 10(4):507–523
- Hansbo A, Hansbo P (2004) A finite element method for the simulation of strong and weak discontinuities in solid mechanics. *Comput Met Appl Mech Eng* 193(33–35):3523–3540
- Hillerborg A, Modeer M, Petersson PE et al (1976) Analysis of crack formation and crack growth in concrete by means of fracture mechanics and finite elements. *Cement Concrete Res* 6(6):773–782
- Kalthoff JF (1985) On the measurement of dynamic fracture toughnesses—a review of recent work. *Int J Frac* 27(3):277–298
- Koh BC, Kikuchi N (1987) New improved hourglass control for bilinear and trilinear elements in anisotropic linear elasticity. *Comput Method Appl Mech Engin* 65(1):1–46

- Lee YJ, Freund LB (1990) Fracture initiation due to asymmetric impact loading of an edge cracked plate. *J Appl Mech* 57:104
- Linder C, Armero F (2009) Finite elements with embedded branching. *Finite Elem Anal Des* 45:280–293
- Liu WK, Hu Y, Belytschko T (1994) Multiple quadrature underintegrated finite elements. *Int J Numer Met Engin* 37(19):3263–3289
- Melenk JM, Babuška I (1996) The partition of unity finite element method: basic theory and applications. *Comput Method Appl Mech Engin* 139(1–4):289–314
- Menouillard T, Réthoré J, Combescure A, Bung H (2006) Efficient explicit time stepping for the extended finite element method (X-FEM). *Int J Numer Method Engin* 68:911–939
- Menouillard T, Réthoré J, Moës N, Combescure A, Bung H (2008) Mass lumping strategies for X-FEM explicit dynamics: application to crack propagation. *Int J Numer Method Engin* 74(3):447–474
- Moës N, Belytschko T (2002) Extended finite element method for cohesive crack growth. *Engin Frac Mech* 69:813–833
- Moës N, Dolbow J, Belytschko T (1999) A finite element method for crack growth without remeshing. *Int J Numer Method Engin* 46(1):131–150
- Nishioka T, Murakami R, Takemoto Y (1990) The use of the dynamic J integral (J') in finite element simulation of mode I and mixed-mode dynamic crack propagation. *Int J Pres Ves Pip* 44:329–352
- Rabczuk T, Song JH, Belytschko T (2009) Simulations of instability in dynamic fracture by the cracking particles method. *Engin Frac Mech* 76:730–741
- Ravi-Chandar K (2004) *Dynamic fracture*. Elsevier, Amsterdam
- Réthoré J, Gravouil A, Combescure A (2005) An energy-conserving scheme for dynamic crack growth using the extended finite element method. *Int J Numer Met Engin* 63:631–659
- Rosakis AJ, Freund LB (1982) Optical measurement of the plastic strain concentration at a crack tip in a ductile steel plate. *J Engin Mater Technol(Transactions of the ASME)* 104(2):115–120
- Rozycki P, Moës N, Béchét E, Dubois C (2008) X-FEM explicit dynamics for constant strain elements to alleviate mesh constraints on internal or external boundaries. *Comput Method Appl Mech Engin* 197(5):349–363
- Song JH, Areias PMA, Belytschko T (2006) A method for dynamic crack and shear band propagation with phantom nodes. *Int J Numer Method Engin* 67:868–893
- Stolarska M, Chopp DL, Moës N, Belytschko T (2001) Modeling crack growth by level sets in the extended finite element method. *Int J Numer Method Engin* 51:943–960